Strategies for object polarization and their role in electrosensory information gathering

IOP Publishing Journal Title
Journal **XX** (XXXX) XXXXXX https://doi.org/XXXX/XXXX

Strategies of object polarization and their role in electrosensory information gathering.

Angel A. Caputi[1] and Pedro A. Aguilera[1]

[1] Departamento de Neurociencias Integrativas y Computacionales Instituto de Investigaciones Biologicas Clemente Estable, Av. Italia 3318, Montevideo, Uruguay. CP 11600

E-mail: caputiangelgmail.com/ acaputi@iibce .edu.uy

Received xxxxxx
Accepted for publication xxxxxx
Published xxxxxx

Abstract

Weakly electric fish polarize the nearby environment with a stereotyped electric field and gain information by detecting the changes imposed by objects with tuned sensors. Here we focus on polarization strategies as paradigmatic bioinspiring mechanisms for sensing devices. We begin this research developing a toy model that describes three polarization strategies exhibited by three different groups of fish. We then report an experimental analysis which confirmed predictions of the model and in turn predicted functional consequences that were explored in behavioral experiments in the pulse fish *Gymnotus omarorum*. In the experiments, polarization was evaluated by estimating the object's stamp (i.e. the electric source that produces the same electric image as the object) as a function of object impedance, orientation, and position. Signal detection and discrimination was explored in *G. omarorum* by provoking novelty responses, which are known to reflect the increment in the electric image provoked by a change in nearby impedance. To achieve this, we stepped the longitudinal impedance of a cylindrical object between two impedances (either capacitive or resistive). Object polarization and novelty responses indicate that *G. omarorum* has two functional regions in the electrosensory field. At the front of the fish, there is a foveal field where object position and orientation are encoded in signal intensity, while the qualia associated with impedance is encoded in signal time course. On the side of the fish there is a peripheral field where the complexity of the polarizing field facilitates detection of objects oriented in any angle with respect to the fish´s longitudinal axis. These findings emphasize the importance of articulating field generation, sensor tuning and the repertoire of exploratory movements to optimize performance of artificial active electrosensory systems.

Keywords: electric fish, object's stamp, gymnotiformes, mormyroidea, multifrequency analysis, electrotomography.

1. Introduction

Weakly electric teleosts provide bioinspiration for artificial electrosensing devices [4-5, 19-24, 79, 90-92]. They are excellent models for understanding how active senses work. These animals generate an electric field that is modified by the impedance of the surrounding media and stimulate cutaneous receptors [64-66]. Thus, the self-generated electric fields serve as a carrier of electrosensory signals produced by the presence or movement of nearby objects that differ in impedance from water [2, 8, 12, 74].

Movements of both the body and the tail can be used to shape the electric field in two ways: by orienting a region of the body to a target object, and by changing the shape of a conducting body that funnels and shapes the electric field generated by the internal current sources [32, 35, 44, 74]. Therefore, electrosensory carrier generation, body shape control, and body orientation relative to a target object´s location are different ways of actively controlling the electric image of a region of interest in the fish's surroundings [32, 35] (however, the term "active" has been traditionally reserved for the ability of generating the carrier energy since its introduction by Bennett and Grundfest [17]).

Due to the decay of the carrier field intensity as a power law of the distance from the fish, this is a short-range sensory modality [12, 44, 45, 68, 75]. The electrosensory field consists of a "bubble" that moves and changes shape with the fish's body [68, 71, 75, 95]. Within this bubble the electric field acts as a carrier of electrosensory signals holistically treated as an electric image of the surroundings by a sensory mosaic. This mosaic shows a high density and variety of electroreceptors around the mouth, where an electrosensory fovea has been described [7, 43, 44, 51, 101].

Electric organ (EO) discharges (EODs), body plan, and receptor responsiveness evolutionarily converged on one of

three electrolocation strategies that may be summarized as: a) pulsed EOD with carangiform locomotion, b) continuous sinewave-EOD with culteriform locomotion, and; c) pulsed EOD with culteriform locomotion.

In pulse Mormyroidea the EO is concentrated in the tail peduncle and discharges a brief pulse [14, 58]. The tail-body angle varies widely during carangiform swimming movements causing large asymmetries in the electrosensory field and therefore changes in electric image [80, 86].

In wave fish the EO is distributed along the body and the EOD consists of a continuous sinewave-like temporal waveform (*Gymnarchus niloticus* [52, 60, 64] from Africa; and Apteronotidae and Sternopygidae [6, 53, 96] from America). In these species, the body adopts a "torpedo-like" shape which is propelled back and forth by a long fin acting as an Archimedes screw (culteriform locomotion) while swimming direction is driven by smoothly bending the body which also causes changes in the electric image [94].

In pulse Gymnotiformes (Rhamphichthyidae, Hypopomidae and Gymnotidae [6, 39-41, 84-85, 100]) the EOD is sum of brief pulsatile waveforms emitted by different regions of the EO driven by a common command. In both pulse and wave Gymnotiformes, waveforms exhibit different time courses and power spectral densities, and are sequentially activated, with a brief lag time, moving from head to tail [6 ,39-41, 73, 81-82, 84-85, 93, 100]

These three strategies may bioinspire different designs of man-made electrosensing devices. This paper explores these strategies in the active electric sense using a toy analytical model and experimentally tests hypotheses derived from the model in a species of pulse Gymnotiformes that exhibits the most complex strategy. This experimental analysis is based on the study of the object's stamp (e.g. the equivalent source of a polarized object [25, 37, 53-54, 74]) as a function of impedance, orientation and position, and also in the evaluation of a reflex-like behavior triggered by a change in stamp (novelty response [1, 33]).

Using theoretical and experimental approaches we found a functional distinction between two electrosensory field zones. At the rostral region of the electrosensory field there is a foveal field in all weakly electric fish (analogous to the foveal field of human vision, tip of the fingers in touch, or the tongue in oral exploration). In this field, the time course of object polarization depends on object impedance, and the strength of polarization depends either on other characteristics of the object (volume and shape), or on the spatial relationship between the object and the fish (position and orientation). In contrast, on the sides of the body, there is a peripheral field in which both strength and time course of object polarization vary differently in the three strategies. We conclude that these strategies may inspire different types of devices such that polarization strategy can be adapted to optimize object discrimination and recognition (including an object's intrinsic, e.g. volume, impedance and shape, and contextual properties, e.g. position, orientation, and movement) depending on the intended function.

2. Methods

This study was carried out in three stages. First, we explored the polarization strategies shown by different fish taxa. We used a toy model to illustrate the main commonalities and differences between these strategies. Second, we experimentally study the most complex strategy as it is a general case which includes the other two as particular cases. This experimental analysis was based on the study of the changes in an object's stamp [25, 37, 53, 74] with impedance, orientation and position. Third, we explored some functional differences in object discrimination using a well-known stereotyped behavior triggered by sudden changes in the electrosensory image [1, 33, 75].

2.1 Modelling of the three polarization strategies

To explore the differences between polarization strategies we used a very simple model validated in most physics textbooks [59, 72, 74]. Although this toy model lacks the complexity introduced by body shape, it clearly illustrates the differences between the fields emitted by a single localized source (Mormyroidea), various sources emitting continuous waves of a single frequency (mormyriform and gymnotiform wave species), and various sources emitting different pulsatile waveforms (pulse Gymnotiformes).

The model consists of two hemispaces: one with the conductivities of water (σ_w) for the object's side, and the other with a much higher conductivity (σ_s) for the source's side. On the most conductive side, electric poles inject currents of intensity I_i at point (x_i, y_i, z_i). Mimicking an EOD, the number of poles was always even and aligned in one direction (either parallel or perpendicular to the hemispace limit). The sum of injected currents was zero.

In the absence of objects, the potential on the objects' side ($\Phi_0(t,x,y,z)$) can be calculated as in [72]:

$$\Phi_o(t,x,y,z) = \frac{1}{2\pi(\sigma_s+\sigma_w)} \bullet \sum_1^n \frac{I_i(t,x_i,y_i,z_i)}{d_i(x,y,z)} \quad (1)$$

where d_i is the distance between each source and the point (x, y, z). The field vectors were digitally estimated by subtraction of consecutive points at dimensions x, y and z.

Current sources and sinks were either aligned parallel or perpendicular to the hemispace separation plane, emulating the field generation either to the side of or in front of the fish body, respectively. Emulating the strategy of Mormyroidea, a single sinewave current cycle was applied between two points on the "fish's side" (one sink and one source separated by two arbitrary units). Emulating the strategy of wave fish, sinewaves of the same frequency were applied between 6 aligned current poles (each separated by 2 units) with a progressive time lag (the closest pole is 2 arbitrary units from the hemispace limit). Emulating the strategy of pulse Gymnotiformes, 6 similarly-located poles emitted pulsatile waveforms, each consisting of a Hanning-windowed single sinewave cycle with a different frequency, phase, and amplitude.

2.2 Experimental study in pulse gymnotiforms.

Experiments were carried out using five fish of the species *Gymnotus omarorum* (unknown sex, 10.5 to 11.8 cm long). Fish were collected in the wild with permission of the Ministry of Agriculture and Fisheries (Direccion Nacional de Recursos Acuáticos, Uruguay). All experiments were approved by the ethics committee of the Instituto de Investigaciones Biológicas Clemente Estable, Uruguay (IIBCE 001/03/2011). After capture, fish were maintained in individual tanks (with water at 18 ºC and conductivity either 80 or 130 μS/cm) in the animal care unit of the IIBCE and fed ad libitum with insect larvae. During the experiments fish were placed in a mesh pen (1.5 cm width, 12 cm length, 10 cm height) at the center of a tank (48 x 28 cm) filled up to 7 cm with either 80 (2 fish) or 130 μS/cm (3 fish) water. No experimental procedure caused harm or major stress to the animals. No chemical treatments were employed. After the experiments the fish were returned to the animal care unit.

2.2.1 Experimental procedures. In a first approach, we experimentally confirmed the accuracy of the method for calculating object's stamp. For this purpose, the Thevenin equivalents of the scene (electromotive force, E_s and series resistance, R_s) were estimated at a given object location by measuring the current and voltage between the cylindrical probe's bases while loading it with different resistors.

Secondly, we verified toy model predictions by evaluating the stamp of objects loaded either with resistive or capacitive impedances at different positions and orientations. While the E_s was directly estimated at each point by measuring the drop of voltage across the cylindrical probe's bases in the presence of a 2.5MΩ shunting resistor, the stamp (ε) was calculated after the impedance of the object was switched to another value (either a short circuit, or a resistor of 10 or 100 kΩ, or a capacitor of 6, 9, 16 and 22 nF). In these experiments the object was stationary for five seconds before and after stepping the stamp value, and then moved to another point in a lattice grid of pre-programed exploration sites on a horizontal plane passing through the fish body. The centre of the object was positioned at each point using an XY plotter commanded by the digital-to-analog port of a Datawave ® interface. In each run, the axis of the object was manually placed on the horizontal plane either parallel or perpendicular to the fish's body axis and its impedance was switched from 2.5MΩ and the chosen impedance. A home-made computer program was used to control the XY movement and to activate a reed relay to switch the load impedance.

Finally, in 4 fish, we tested behavioural discrimination between two stamps of an object positioned at different points and orientations in the electrosensory field. We evaluated discrimination with the novelty response, a native reflex-like orienting behaviour consisting of a sudden reduction of the inter-EOD interval after the occurrence of a novel electrosensory stimuli in the electrosensory field [1, 30]. In these experiments the object was stationary for 30 seconds before stepping the stamp value, was held in position for another 5 seconds, and then moved to another randomly chosen position in the lattice grid. Each position was explored by the same change in impedance 3 to 5 times.

Objects were plastic cylinders either of 17 mm length and 8 mm diameter (3 fish) or 30 mm length and 8.8 mm diameter (2 fish), with conductive bases, but non-conductive curved surfaces. These objects are frequently used for exploring electroreception [1, 33, 98] because their longitudinal impedance can be modified at will by connecting the bases through discrete elements (e.g. resistors, capacitors, and their combination). Their easy construction, well-defined shape and controllable longitudinal impedance facilitate the study of the electric image as a function of different features of an object (including impedance, volume, shape, position and orientation with respect to the fish axis).

Furthermore, in these kinds of objects, the stamp (the equivalent electric source to cause the same perturbation of the self-generated field) can be evaluated experimentally. To calculate the stamp, we simultaneously recorded the voltage between the object's bases and the current through the object. For voltage recordings, each of the carbon bases were connected to the high impedance input of a differential amplifier (gain x100, bandpass 10-10kHz, AM systems 1800). For current estimation, we recorded the drop of voltage (gain x1000, bandpass 10-10kHz, AM systems 1800) across a 2 kΩ resistor that was connected by one end to one of the bases of the cylinder and by the other to the load impedance. Thus, the impedance along the object always had two components in series, a 2kW resistor and another element whose impedance was defined for every experiment. A pair of electrodes placed on the tank walls, facing the head and tail, was connected to a third amplifier (gain x100, bandpass 10-10kHz, AM systems 1800) to evaluate the timing of the EOD. Amplifier output, position of the XY plotter, and timing of the switch were sampled at 50 kHz (Datawave ®).

2.2.2. Signal analysis. We used in-house code to evaluate data files containing object position, voltage and currents generated by the EODs across the object, and EOD timing from 5 seconds before to 5 second after switch activation.

First, we identified the timing of the positive peak of the head to tail EOD with respect to the timing of the switch.

Second, the waveforms of the voltage and current at each explored point were estimated by averaging 8-10 EODs before and after each impedance step.

Third, voltage waveforms were plotted vs. current waveforms to verify whether they were proportionally (as expected for resistive loads) or non-linearly (as expected for capacitive loads) related.

Fourth, the equivalent electromotive force of the scene (*Es*) and the internal resistance (*Rs*) was estimated in the runs where we used resistive loads. In this case, the amplitude of the recorded current linearly decays with the sum of internal (*Rs*) and load (*Ro*) resistances, but the voltage increases. *Es* is the voltage drop across the object's bases when *Ro* approaches infinity and current approaches zero. Voltage recordings obtained with *Ro* = 2.5 MΩ were associated with negligible currents. Thus, these voltage recordings were considered a good proxy for E_s. When plotting voltage vs current, the maximal values were aligned and well fitted by

a descending line with slope -*Rs*. Thus, each point of the lattice grid *Rs* was evaluated as the quotient between two points that defines the line, one obtained loading the object with *Ro*=2.5 MΩ and the other with *Ro*=2kΩ.

Fifth, the stamp of the object was calculated by taking into account the longitudinal resistance of the water displaced by the cylinder:

$$Rw = \frac{\rho.length}{\pi.radius^2} \qquad (2)$$

For a resistive load (R_0):

$$\varepsilon = E_s \bullet \frac{R_o - R_w}{R_o + R_s} \qquad (3)$$

More generally the three variables measured in the experiments (E_s, R_s *and* I_{obj}) allowed us to calculate the stamp in any condition (see results):

$$\varepsilon = E_s - I_{obj} \cdot (R_w + R_s) \qquad (4)$$

Sixth, in 4 experiments we tested stamp discrimination stepping from a high resistance (2.5 MΩ) to a low reactance (2kΩ in series with a shunt, another resistance or a capacitance). The increment of the stamp was calculated as:

$$\Delta\varepsilon = -I_{obj} \cdot (R_w + R_s) \qquad (5)$$

We evaluated the amplitude of the novelty responses (*ANR*) as the maximal reduction of the inter-EOD interval in the 4 EODs following the increment in stamp. We normalized this value by the median of the 5 intervals before the change in stamp (I_{before}):

$$ANR = \frac{(I_{before} - I_{minimal})}{I_{before}} \qquad (6)$$

3. Results

3.1 Theoretical analysis of polarization strategies in weakly electric fish.

We used a toy model consisting of two hemispaces of very different conductivity to evaluate the electric field generated by: a) a unique localized source, b) multiple sources emitting sinewaves of the same unique frequency but different amplitude and phase, and; c) multiple sources emitting different waveforms.

The first strategy is represented in Mormyroidea. They emit a brief discharge driven by a neural command occurring irregularly [48]. This command synchronously activates hundreds of electrogenic cells densely packed in a short EO at the tail peduncle [14, 18, 36, 48]. This can be mimicked by a single dipole.

The toy model suggests that the electric field generated in this condition has a constant direction all along the time course of the EOD (Fig.1). Thus, it can be predicted that object polarization will tend to be maximal when field direction is perpendicular, and minimal when it is orthogonal to its main axis. Thus, taking into account both dipole orientations, mimicking the effects of the EOD on the rostral and lateral regions of the body, the toy model suggests that mormyrids show the same polarization mechanism in all object positions of the electrosensory field. (Fig.1).

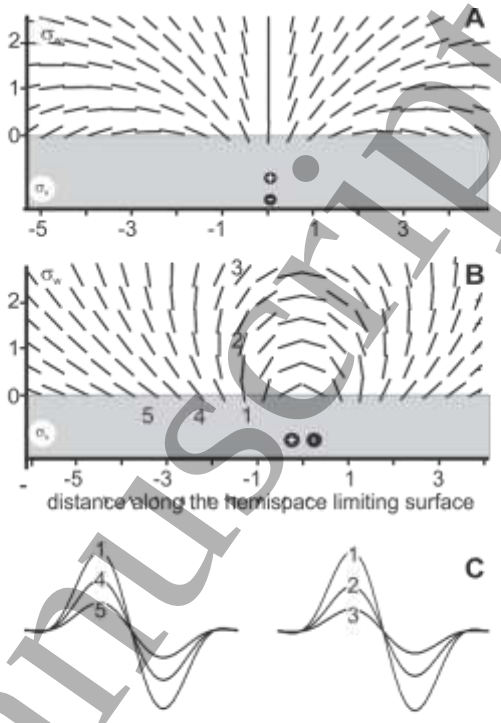

Figure. 1. Toy model; Mormyroidea. The lines represent the trajectory of the field vector head generated at equally-spaced positions in the low-conductive hemispace (σ_w) by two poles (black circles) located on the high-conductive hemispace (σ_s). The grey background corresponds to the intensity of the field (normalized to the highest field value). A. The poles are aligned perpendicularly to the limiting plane. B. The poles are aligned in parallel with the limiting plane. C. Time courses of the field at the sites indicated by the numbers in B. Units are arbitrary.

Wave fish emit a permanent sinewave-like field resulting from the summation of regional EO activities of the same frequency but delayed in phase from rostral to caudal regions of the body. When the sources are aligned perpendicular to the separation between a high and low conductive hemispace, the polarization fields have a nearly constant direction and its time course is similar for all positions. Since the sources are relatively far from the object, the field (e.g. the weighted sum of the effects of all sources at the object position) has about the same time course everywhere and differs only in amplitude and polarity (Fig 2 A).

When sources are aligned parallel to the hemispace limit, the phase lag causes a rotation of the electric field on the fish side [5/, 85bis]. The loops in Figure 2B illustrate the trajectory of the field vector head around a different point of application. The norm of the vector depends on phase lag and location relative to the source sites. Near the hemispace limit, the root mean squared (rms) value of the field shows two maxima close to the ends of the series of poles, and decays with distance (Fig 2C). Thus, the model suggests that the polarization of an object placed on the side of a wave fish will follow a time course characterized by a sinewave of the

same frequency, but a phase- and distance-dependent orientation and intensity.

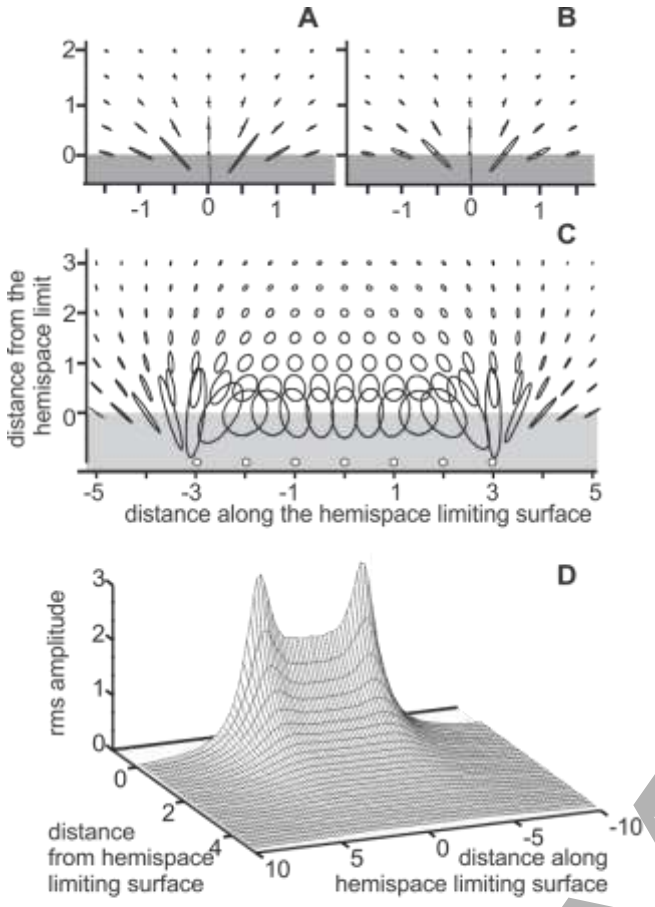

Fig. 2. Toy model; wave fish. The lines represent the trajectory of the field vector head generated at equally-spaced positions in the low-conductive hemispace (σ_s) by multiple poles located on the high-conductive hemispace (σ_i). A and B the poles are aligned perpendicularly to the limiting plane. C. The poles are aligned in parallel with the limiting plane. D. rms value of the field value. All units are arbitrary.

Finally, pulse Gymnotiformes possess complex electric organs distributed along the caudal 90% of the body. In these fish, different regions of the EO are sequentially activated by a pacemaker firing at a regular rate of tenths of Hz. In each EO region the electrocytes show characteristic innervation patterns, size, membrane properties and density [31, 36]. The discharge is the sum of regionally-emitted pulses of distinct time courses with different, but partially overlapping, power spectral densities, and different phase spectra [36/-38/, 74/-75/, 89/]. To mimic this strategy, we used a series of sources with different waveforms consisting each of a single sinewave cycle of different frequency, phase, and amplitude, windowed through a Hanning profile with an effective duration of about one cycle.

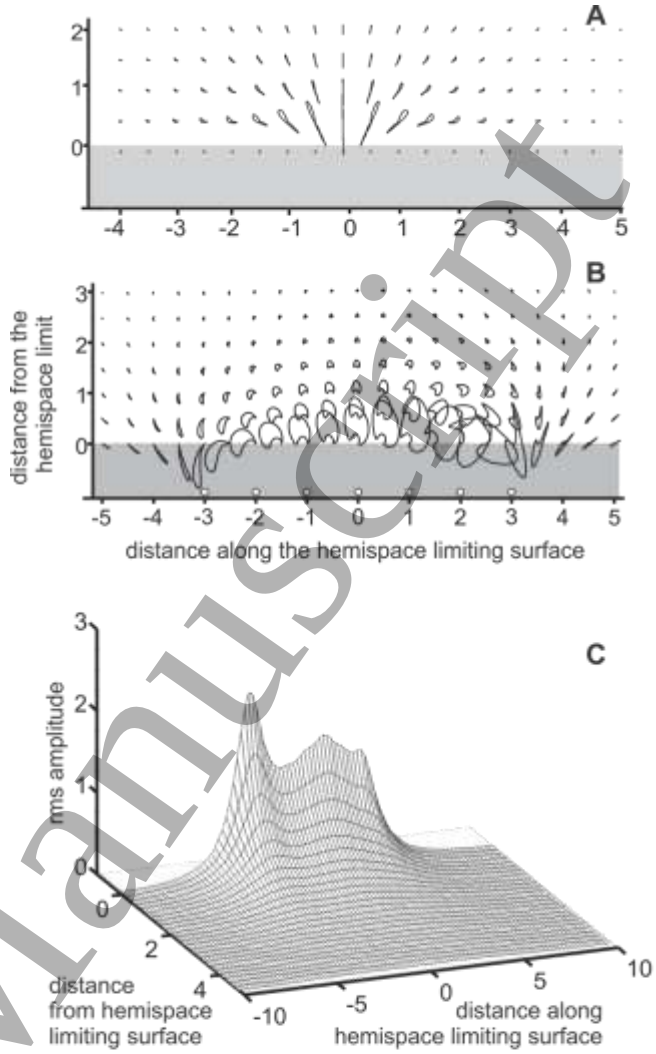

Fig. 3. Toy model; pulse Gymnotiformes. A and B: The field is represented at each site by a moving point indicating its instantaneous magnitude and direction angle (with respect to a fixed application point at the evaluated site). The lines represent the trajectory of the field vector head generated by multiple poles emitting distinct waveforms and located on the high-conductive hemispace (σ_i) at equally-spaced positions in the sources plane in the low-conductive hemispace (σ_s) A. the poles are aligned perpendicularly to the limiting plane. B. The poles are aligned in parallel with the limiting plane. C. rms value of the field value. All units are arbitrary.

As in wave fish, when the sources are aligned perpendicular to the separation between the hemispaces, the polarization fields have a nearly constant direction, and its time course is similar for all positions, but different from the other two strategies, when the sources are aligned along the hemispace limit, the field follows very complex trajectories (Fig. 3B). Close to the wall, the field amplitude also shows a complex profile (Fig 3C).

Here we can hypothesize that in the two last strategies there are functional differences between two regions in the electrosensory field (defined by analogy to the visual field as the region of space in which an object has a significant effect on sensory processing). In analogy to the retina, taking into account where the image of a small object located in the electrosensory field maps onto the sensory mosaic, we define: 1) a foveal electrosensory field where the electric

field has a coherent waveform and attenuates in magnitude, and which orientation angle increases with distance from the fovea, and; 2) a peripheral electrosensory field where the time course and direction of the polarization field is different for every object position to the sides of the fish.

3.2. Experimental evaluation of object polarization

The aim of this section is to report the experimental tests of the hypotheses on object polarization derived from the toy model analysis in pulse gymnotiforms. Results from all studied fish were qualitatively similar and support the hypotheses. We exemplify them with data obtained in individual fish in each plot. Consistency is illustrated by showing experiments from different animals.

3.2.1. The concept of object's stamp. To evaluate object polarization strategies, we applied the concept of "object stamp". One must recall here that the electric image of an object can be reproduced in the absence of the object by multiple discrete sources placed on a surface, casting object shape. Therefore, for a given object, we have defined the concept of the object's stamp (or imprint, impronta in Spanish, or empreinte in French [37, 74]) as the electromotive force of the electric source (or a distributed set of sources) that generates the same image on the fish's skin in the absence of the object.

We used object probes consisting of a nonconductive cylinder with conductive bases ([1, 33, 83, 97-98]). To show the validity of the method employed to evaluate polarization of these objects, we first show how to experimentally evaluate the scene parameters that serve an object's polarization, and second that theoretical predictions of the stamps of these objects can be accurately calculated for any impedance connected between the cylindrical probe bases.

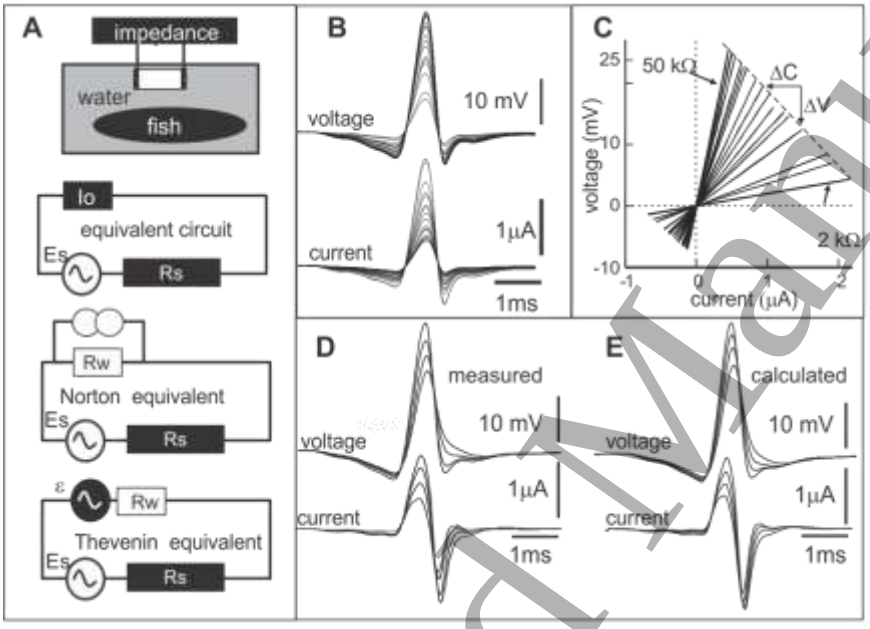

Figure 4. The concept of stamp. A. The setup and the Thevenin-Norton equivalent circuits. B. Overlapped traces correspond to the voltage and current across the bases of a cylindrical probe recorded while loading it with different resistors. C. Voltage vs. current plots for each resistive load. The absolute value of the slope of the dashed line (e.g. $\Delta V/\Delta C$) and the ordinate crossing correspond, to *Rs* and *Es*, respectively. D. Comparison between calculated (left) and measured (right) current and voltage waveforms for 4 capacitance values (6, 9, 15, and 22 nF) in series with a resistor of 2 kΩ. Object size: 4.4 mm radius and 30 mm length. Position: 5 mm apart from the snout. Qualitative results were similar in all five fish.

The concept of stamp is illustrated with experimental data obtained with a cylinder of 8.8 mm diameter and 30 mm length loaded with a resistance of 2 kΩ in series with a rheostat to vary load resistance (Fig. 4).

In the five fish, our data confirm that the whole scene can be considered a linear system. This means that the Thevenin-Norton theorem is applicable, which allows us to think of the system as two simple electric sources (Fig 4A). On one hand, one should consider the object connected to the scene through its cylindrical bases. This can be represented by the stamp of the object and an impedance equivalent to the resistance of the water cylinder displaced by the object (*Rw*). On the other hand, the scene (including the fish and the tank) can also be represented by an equivalent electromotive force (*Es*) and a resistance (*Rs*). Each part (object or scene) can be represented by a resistance connected in series to a pure voltage source (ε) in the Thevenin version, or in parallel to a pure current source in the Norton version (Fig.4). The almost identical time course of the voltage drop and current (top and bottom in Fig 4B, respectively) across the cylindrical object bases, and their reciprocal increment in amplitude when the object resistance is modified, support linearity. For each load resistance, time courses were proportional point to point with a slope equal to the load resistance (Fig. 4C). The scene equivalent resistance (R_s) corresponds to the slopes of the lines of the voltage-current plot obtained at any point of the waveform. However, as current or voltage approaches zero, the accuracy of this calculation is greatly reduced by noise at polarity transitions. To circumvent this drawback, we estimate R_s by line fitting the maximum values of the voltage and current obtained with all resistance values used in each experiment (Fig. 4C dashed line). The ordinate and the abscissa projections of this voltage-current dashed line are the electromotive force of the scene ($E_s(t)$) and the maximal current that the scene can supply through the object,

respectively. Once E_s and R_s were estimated, we were able to calculate and experimentally test the waveform and amplitude of the stamp (ε) for any object impedance. In the case of a pure resistive load (R_0):

$$\varepsilon = E_s \bullet \frac{R_o - R_w}{R_o + R_s} \qquad (3)$$

The validity of the linear assumption when applying the Thevenin theorem was tested by comparing the calculated voltage and time courses of the current and voltage across the cylindrical object when its bases were shunted with a complex impedance. Figure 4D illustrates data from one individual. In these recordings the impedance of the object consisted of a capacitance (C) in series with a resistance (necessary for measuring the current, Rm=2KΩ). Predictions were calculated as follows: the voltage across the object (V_{obj}) is equal to the sum of the voltage across the capacitor (V_{cap}) plus the voltage across the current-measuring resistor:

$$V_{obj} = V_{cap} + I_{obj}.R_m \qquad (7)$$

The stamp ε is the electromotive force that would algebraically summate to the electromotive force of the scene to drive the current I_{obj} through a cylinder of water similar to the probe with a longitudinal resistance Rw to get the same voltage (V_{obj}):

$$\varepsilon = E_s - I_{obj*}(R_w + R_s) \qquad (4)$$

Then the voltage across the capacitor (V_{cap}), the current (I_{obj}) through the cylinder, and the Voltage between the cylinder's bases (V_{obj}) were estimated as:

$$V_{cap} = \frac{e^{-t/\tau}}{\tau} \int_{onset}^{t} E_s \cdot e^{t/\tau} \cdot dt \qquad (8)$$

$$I_{obj} = \frac{1}{R_s + R_m}\left(E_s - \frac{e^{-t/\tau}}{\tau} \int_{onset}^{t} E_s \cdot e^{t/\tau} \cdot dt \right) \qquad (9)$$

Where the time constant (τ) is defined as:

$$\tau = (Rs + Rm) * C \qquad (10)$$

Voltage and current estimations were experimentally confirmed in this way in 4 fish (using 4, 3, 1 and 1 capacitive loads). The coefficients of determination (ranging from 0.90 to 0.96) show a good agreement between theoretical predictions and experimental data.

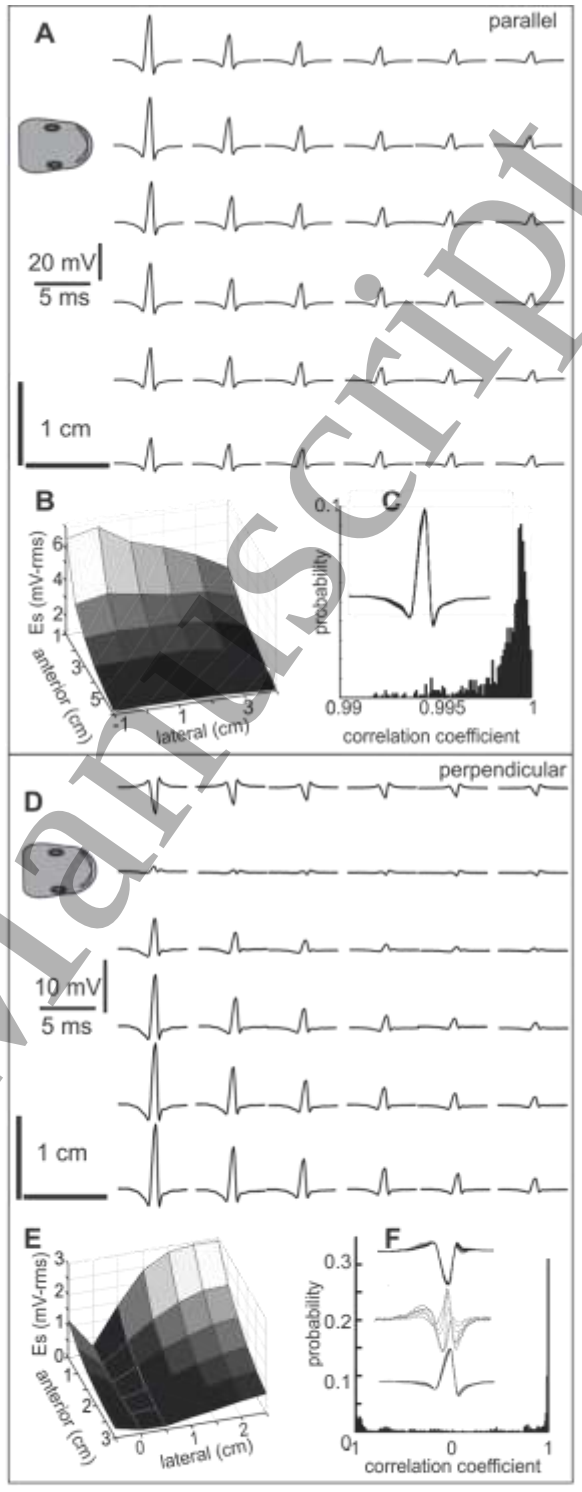

Figure 5. The electromotive force of the scene. A The electromotive force of the scene (Es) is plotted for a lattice grids of points of the electrosensory field in when the axis of the object is parallel to the fish axis. Traces positions are on register to the recording points respect to the fish. B. Surface plot of the rms value of Es shown in A. C. Histogram of the correlation coefficients between each pair of waveforms shown in A.. The inset shows the normalized traces overlapped. D. Es is plotted for a lattice grids of points of the electrosensory field in when the axis of the object isperpendicular to the fish axis. Traces positions are on register to the recording points E. Surface plot of the rms value of Es shown in D. F. Histogram of the correlation coefficients between each pair of waveforms shown in D.The insets show normalized traces overlapped. While those in opposite sides of the midline are mirror images, 5 obtained on the midlineshow different waveform (gray traces) but negligible amplitude.

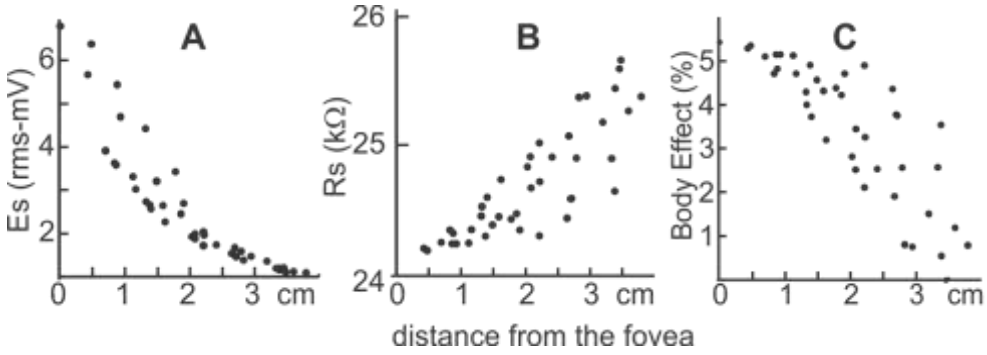

Figure 6. The amplification fringe The parameters of the scene and the effect of the fish body as a function of the Euclidean distance from the fovea. A.Equivalent electromotive force (Es). B. Equivalent resistance (Rs). C. Body effect.

3.2.1. Object stamps at the foveal electrosensory field. Within the foveal field the rms-value of the stamp decayed with distance but the waveform was position independent and typical for each impedance. As the distance from the transversal plane passing through the fovea increases, the field and *Es* decreases (Fig. 5A and B). The literature indicates [72, 75] that effect of orientation is a cosine function of the angle between object and fish axis. Consistently, the field curves laterally causing that the rms-value of *Es* decreases when "seen" by objects oriented parallel to the fish axis (Fig 5A and B) but an increase when "seen" by perpendicularly-oriented objects (Fig. 5D and E). Polarization of objects on each side of the fish axis has obviously opposite polarity (Fig. 5D and F). Interestingly, in most object positions and in both orientations the waveforms of the stamps are similar (Fig. 5A and B). For objects oriented parallel to the fish axis the coefficients of correlation calculated between pairs of recordings were very large (Fig 5). In the case of perpendicularly oriented objects the time course of the stamps of object centered on the fish axis, small differences in centering and orientation due to small fish movements caused large changes in waveform (see noisy traces in the inset of Fig 5F) but the rms-value of these stamps was negligible.In addition to the attenuation of scene electromotive force (Fig 6A) the scene resistance increases as the object moves away (Fig 6B). As *Rs* decays with distance to the fovea, ε decayed more steeply than Es. According to the literature [24, 34, 70, 74] this is a passive effect of the fish body. To evaluate this effect, we defined an index which evaluates the relative difference between ε with a virtual stamp (ε^*) calculated using a constant scene resistance value (Rs^*) measured 10 cm away from the fish.

$$Body\_Effect = \frac{(\varepsilon - \varepsilon^*)}{\varepsilon^*} = \left(\frac{Rs^* - Rs}{(Ro + Rs)}\right) \quad (11)$$

At the fovea where the effect is largest [2, 44] it ranged between 4 and 7% in among the five fish (Fig. 6C).

The stamp waveform is the same for the same capacitance loading a cylinder placed in the foveal electrosensory field. The voltage and current recorded across the probe when a capacitor of 9 nF was connected in series with *Rm* are shown for three object positions in Figure 7. They are very similar in waveform and their amplitudes decay with distance to the fish (Fig 7A and B). This is expressed by the similar loops observed in the current-voltage plots (Fig 7C). Moreover, the normalized loop (Fig. 7D) the time course of the stamps (Fig 7E) and are nearly identical.

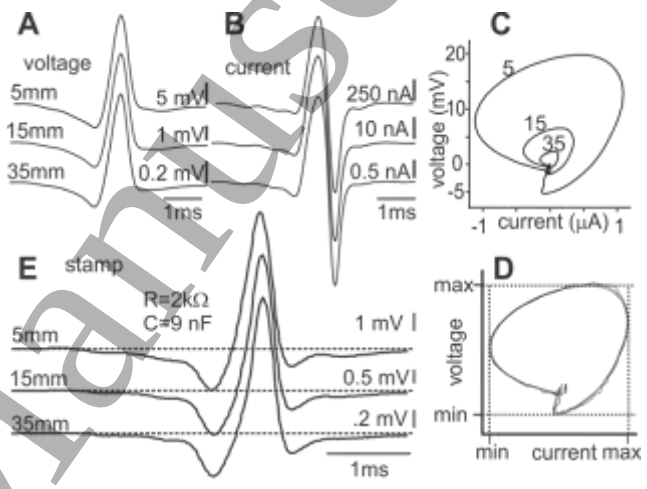

Figure 7. The stamp of capacitive objects in the foveal field. A and B. Voltage and current between the cylinder bases at three different distances from the snout (5, 15 and 35 mm). C. Voltage vs current plots. D. When the plots from C are normalized, loops are identical. E. The stamps of the object at the three distances show a similar time course (traces were normalized, calibration on the side).

3.2.3. Object stamps at the peripheral electrosensory field. In all studied fish the time course and amplitude of the stamp was site-specific on the side of the fish body. We found large variations of the time course of *Es* with the probe's orientation relative to the fish axis. In Figure 8 A *Es* is represented at each object location relative to the fish, the object axis is perpendicular to the fish axis on the right side, and parallel on the left. Consistence between the time courses of the current measured with and object load of 2kΩ and the voltage measured with and object load of 2.5MΩ at the same object positiona and orientation indicates linearity (Fig 8 B and C).

These changes in *Es* are matched by variations in object's stamp (Fig. 9A, B and C). The site-specific variations in time course and amplitude of the object's stamp were associated to changes in rms-value, showing spatial profiles dependent on object orientation and impedance (Fig. 9D to G). Interestingly, while the rms-value of the stamp of an object placed on a line perpendicular to the fish axis decays

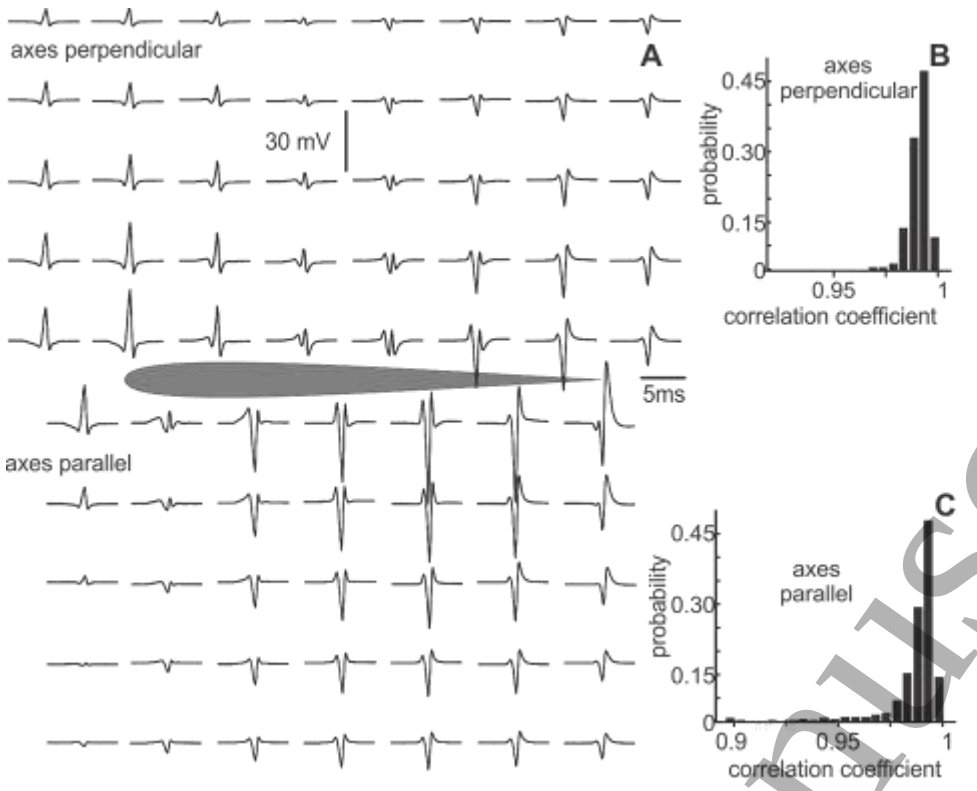

Figure 8. The electromotive force of the scene (*Es*) for each position at the peripheral electrosensory field. A. Each trace is the recorded *Es* as it is "seen" by an object placed at the relative position from the fish body (indicated by the fish silhouette). On the right and left sides of the fish the object was perpendicular and parallel to fish's main axis, respectively. B and C. Distributions of the correlation coefficients between the normalized time courses of the voltage and current through the object when the loads were 2.5MΩ or 2 kΩ respectively at each position in the field. Object and fish axes were parallel in B and perpendicular in C.

with distance, its time course remains relatively similar for both resistive (compare the three top traces in Fig. 9A) and capacitive loads (compare the three bottom traces in Fig 9B).

In addition, the time course of the stamp also varies as a function of the orientation angle at each object position (Fig. 9C).

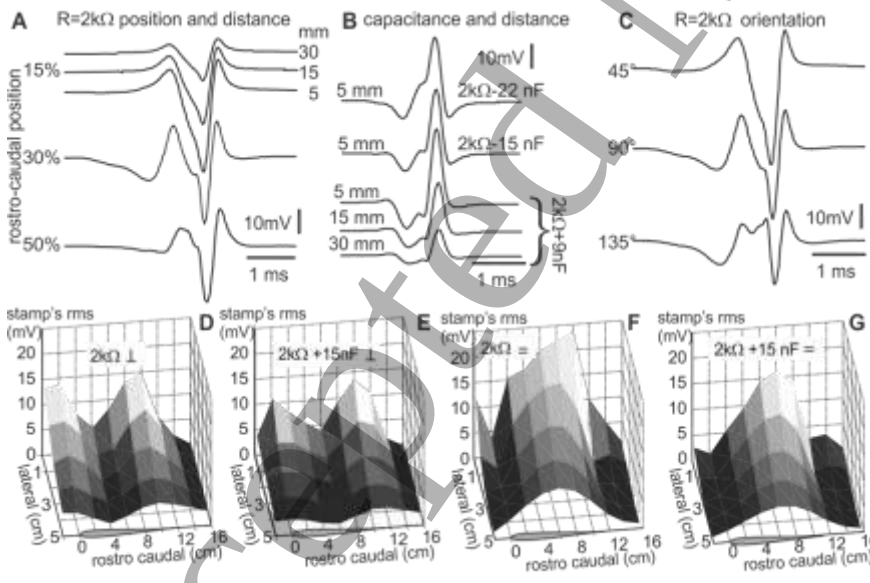

Figure 9. The stamp of the cylindrical probe varies in time course and rms value at the peripheral electrosensory field.

A. Stamp of an object with 2kΩ core impedance at a distance from the snout equivalent to 15, 30 and 50 % of the fish's body length. **B.** Stamp of the same object loaded by either 2 kΩ + 22 nF, 2 kΩ + 15 nF or 2 kΩ + 9 nF impedances. Note the variability in time course with capacitance (upper key bracket). In A and B large changes in amplitude but small changes in time course, were caused by moving the object away from the skin (upper 3 traces in A and low key bracket ib B labelled as 5, 15 and 30mm). **C.** Important changes in time course were observed when the object axis was placed in different orientations (45, 90, 135 degrees) with respect to the main axis of the body. **D to C.** Surface plots of the rms-values of the object's stamps D and E object perpendicular to fish longitudinal axis (indicated with an inverted T, Object load in **D** 2kΩ and **in E** for 2kΩ + 15nF). F and G objects ax es parallel (indicated with an = sign, Object load in **F** 2kΩ and **in G** 2kΩ + 15nF).

3.3. Object detection and discrimination in foveal and peripheral electrosensory fields.

Here we report data that support the hypothesis that the functional roles of foveal and peripheral electrosensory fields are different. We used novelty responses to show that discrimination differs between both electrosensory fields, in particular in the way that they discriminate impedance and in the relative importance of object orientation relative to the fish's main axis.

It is well known that changes in stimulus waveforms are detected by *G. omarorum* when the object is placed within a narrow fringe bordering the foveal region [1, 83]. Here we compared object detection for resistive and capacitive objects over a wide range of the electrosensory field (Figure 10). We provoked novelty responses by changing the reactance of the path between the object's bases from 2.5 MΩ to either a capacitive or a resistive impedance with objects placed at different places of the electrosensory field.

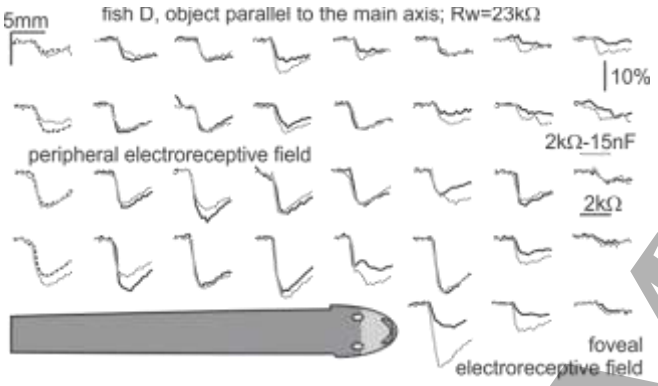

Figure 10. Behavioral exploration of the electrosensory field. Time course of the inter-EOD interval when the object impedance was stepped from 2.5MΩ to 2kΩ (black lines) and from 2.5MΩ to 15 nF in series with 2kΩ (gray lines) at different positions in the field. Not the differences in the foveal field and the similarities in the peripheral field.

Consistent with the example of Fig 10, the novelty responses evoked by steps in the object's impedance at the foveal field are well correlated to the root mean squared value of the change in object's stamp (data from an additional two fish are shown in Fig 11). The increment in stamp (Δε) caused by stepping from 2.5 MΩ to 2kΩ, and from 2.5 MΩ to 9 nF in series with 2kΩ (Fig 11 A and B, respectively) showed no changes in waveform when it was explored with the object placed at different points. However, Δε showed an important decay in rms-value. This decay is a power function of the Euclidean distance from the snout (Fig. 11C). Importantly, the rms- values of Δε resulting from stepping from high resistive to capacitive loads (open symbols, Fig 11C) is shifted to lower values with respect to the curve obtained with a pure resistive step (filled symbols, Fig 11C).

Remarkably, while novelty responses to each type of stimulus increase with the change in stamp's rms value, capacitive impedance caused larger responses than the pure resistive step when the object was at the same site (compare the slope of the lines relating the amplitude of the novelty response to Δε in Fig 11D).While the response to changes only in object resistance showed similar slopes, the responses to the capacitive objects show different slopes depending on capacitance (Fig. 11 E and F). The fact that the amplitude of the novelty response is a linear function of the rms of Δε but with an impedance-dependent slope, indicates that fish is able to discriminate waveform across the foveal electrosensory field.

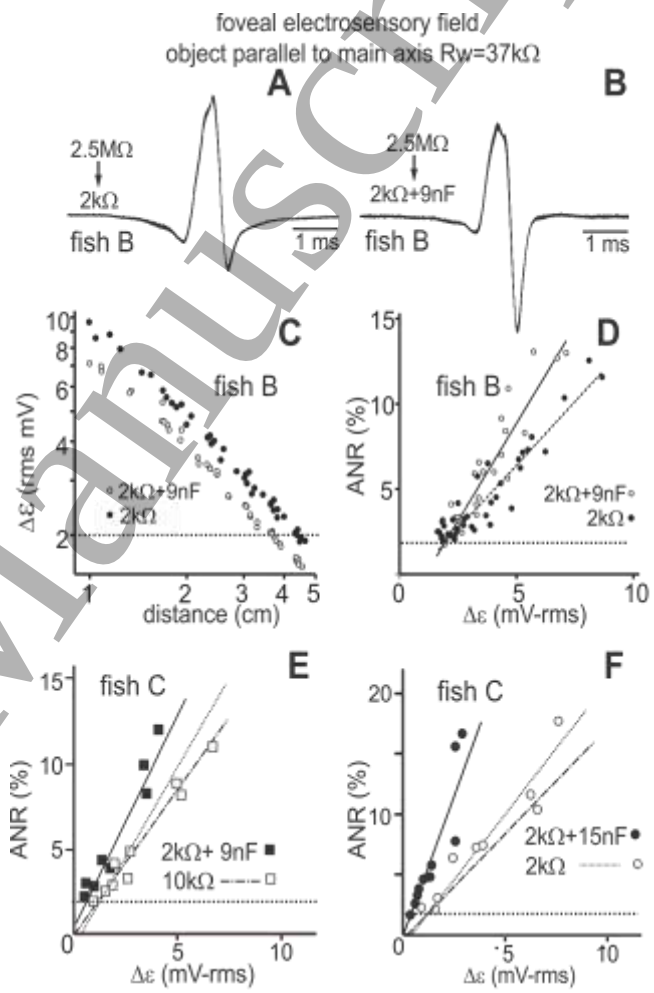

Figure 11. Waveform discrimination at the foveal electrosensory field. A. Twenty two superimposed traces corresponding to the normalized change in the object's stamps when the core resistance changed from 2.5 MΩ to 2 kΩ evaluated at different points of the foveal field. B. Twenty two superimposed traces corresponding to the normalized change in the object's stamps when the core resistance changed from 2.5 MΩ to 2 kΩ+9 nF, evaluated at different points of the foveal field. C. Increment in object's stamp (Δε, rms-value) for the stimulus used to evoke novelty responses shown in D as a function of distance from the fovea (object parallel to the main axis of the fish's body). Note the logarithmic scales and that the capacitive load causes lower values than resistive ones. D and E. Amplitude of the novelty response (ANR) as a function of the increment in Δε when the impedance was stepped from 2.5 MΩ to 2 kΩ+9nF and from 2.5MΩ to 2kΩ (D and E were obtained in a different fish) F. ANR as a function of the increment in stamp rms-value when the impedance was stepped from 2.5 MΩ to 2 kΩ +15nF and 2.5 MΩ to 10 kΩ +15nF in the same fish as in E. To facilitate comparison, the line fitting the white squares (10kW) in E was represented in F and the.line fitting the white circles (2kW) in F was represented in G

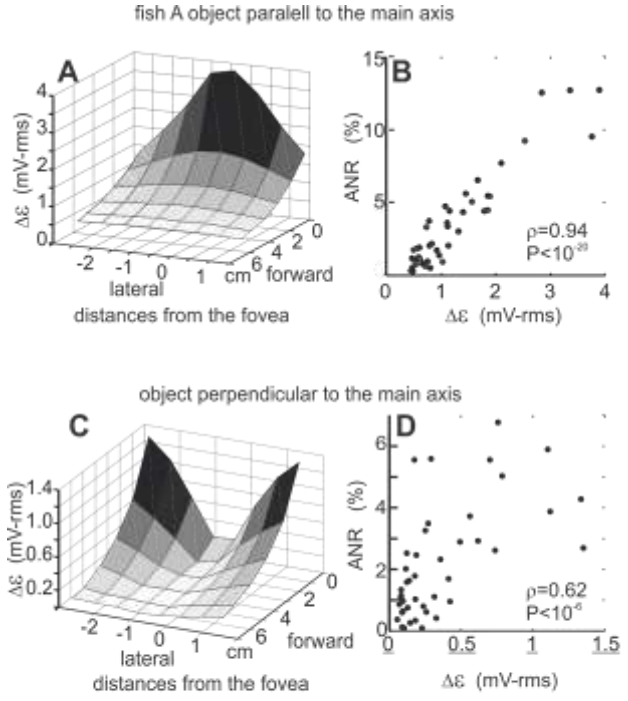

Figure 12. The importance of object orientation at the foveal electrosensory field. A and C. Spatial distribution of the rms-value of the change in stamp (Δε) used to trigger the novelty response. B and D. Amplitude of the novelty response evoked at different points of the foveal electrosensory field by the same step in resistance (2.5MΩ to 2kΩ) plotted as a function of the increment in stamp (Δε). The object was placed parallel to the main axis of the fish (A and B) and perpendicular (C and D) to the main axis of the fish

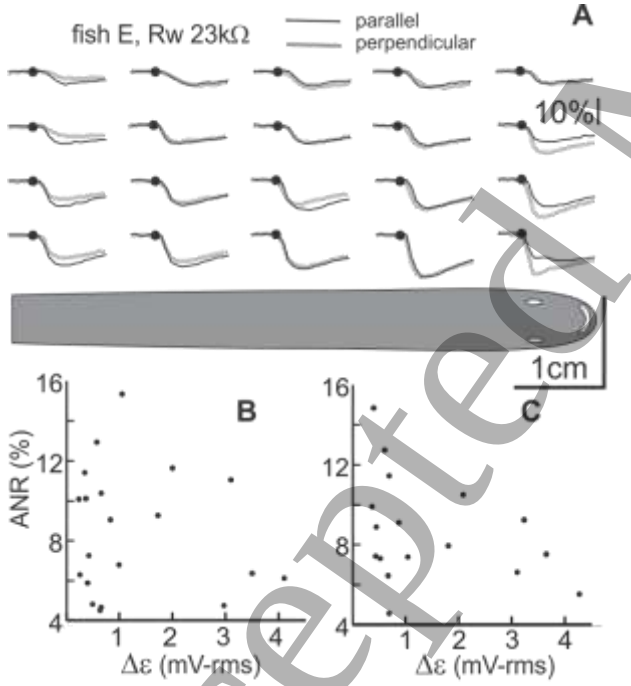

Figure 13. Novelty responses at the peripheral field A. Time course of the inter-EOD interval when the object impedance was stepped from 2.5MΩ to 2 kΩ. The object was placed parallel (black traces) or perpendicular (gray traces) to the fish axis. The black dots indicate the position of the object relative to the fish and the timing of the step. Note the similarity of the response for the two object's orientations and the same object position Amplitude of the novelty response as a function of the increment in stamp B parallel and C perpendicular.

The amplitude of the novelty response depends on the distance of the object from the fovea and on the alignment between the polarizing field and the object axis (Fig.12).

The novelty responses evoked by resistance steps in the object resistance follow a linear function of Δε (Fig. 12B). Nevertheless, there was a weaker correlation when the object was perpendicular to the main fish axis in the foveal field (Fig. 12D) probably because of the smaller Δε caused by the resistance step at orthogonal positions of object and fish axes, and also because of the exceptions shown in Figure 5F.

On the side of the fish Δε showed large variations when object axes were placed orthogonally. However, no significant differences were found in the amplitude of the novelty response obtained by similar changes in stamp when the object was placed at the same points in the peripheral field (Fig. 13A). In addition, we found poor correlation coefficients between the increment in stamp amplitude and the amplitude of novelty responses (Fig. 13B and C).

However, the plot of the amplitude of the novelty response as a function of the increment in rms value of the object's stamp was well fitted by a straight line when considering those object locations along a line perpendicular to the main axis only.

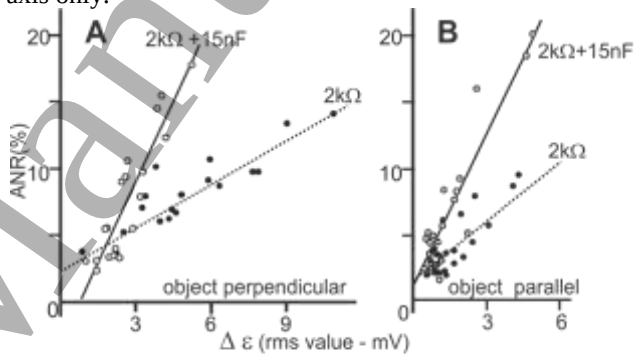

Figure 14. Waveform discrimination at the peripheral field. Novelty responses were evoked by stepping the object impedance from 2.5MΩ to 2kΩ and from 2.5MΩ to 2kΩ+ 15 nF. The object was placed orthogonal (A) and parallel (B) to the fish axis at different points on the same line perpendicular to the skin (where the stamp of the object has a similar time course, see Fig. 9).

Capacitive loads provoked novelty responses of larger amplitude (Fig. 14). The differences in the steepness of the slope of the fitting lines indicate that differences in stamp waveform caused by resistive and capacitive object impedances are similarly discriminated when the object was perpendicular (Fig 14A), and also when parallel (Fig 14B) to the fish's main axis.

The data overlap near the threshold value. Therefore, to pinpoint whether there is waveform discrimination up to the limit of the electrosensory field, we explored whether changes in waveform with no changes in the rms value of the stamp caused novelty responses along lines perpendicular to the skin. We found that a step in impedance between a resistive (adapted for stamp matching in each fish) and a capacitive load (2 kΩ plus 9 nF in series) caused weaker responses as distance increased, and the waveform difference was detected across the entire electrosensory field (Fig. 15).

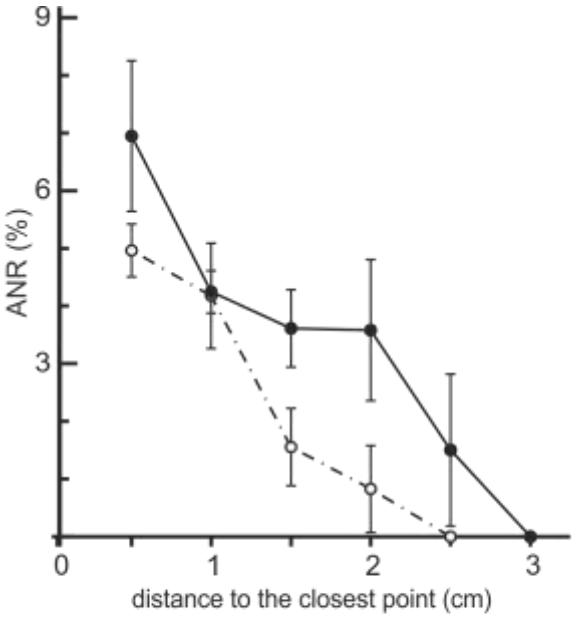

Figure 15. Waveform discrimination as a function of distance. Circles and bars correspond to the mean and standard deviation values of the amplitude of the novelty response evaluated in three fish as a function of distance to the closest point in the skin. Filled symbols with solid lines correspond to the experiments on the side of the fish at 25% distance from the snout. Open symbols and dashed dot lines correspond to the experiments on the foveal field along the main axis of the fish.

4. Discussion

4.1 The toy model shows three polarization strategies

The toy model illustrates the proximal causes (e.g. the subservient mechanisms) and suggests potential ultimate causes (e.g. the usefulness) of polarization differences among fish taxa, providing knowledge for suitable design of artificial electrosensory agents, and bioinspiration for expanding their functionality.

The toy model indicates that when the sources are aligned perpendicular to the hemispace limit, the field varies in amplitude and polarity, but not in direction, for all polarization strategies. When the instantaneous field is represented by a point indicating its magnitude and direction angle (with respect to a fixed application point at the evaluated site), its trajectory during the EOD describes a very narrow loop (Figs 1 to 3). Experimental and modelling results [2, 6, 44, 81] show that this is a common feature in all species of weakly electric fish at the perioral region. This region possesses the highest density and variety of receptors, and is most suited to explore field changes with high spatial resolution, and it has been likened as an electrosensory fovea [7, 44, 51, 101].

When the sources are aligned perpendicular to the hemispace limit, the model distinguish three possible cases. This suggests that evolution has converged onto one of three strategies for the polarization of nearby objects expressed in a) pulse Mormyriformes, b) wave Gymnotiformes, and; c) pulse Gymnotiformes.

4.1.1. Mormyriformes. In this case, a single source represented by two poles. The toy model shows that the polarization field replicates the time course of the emitted waveform. Across the entire electrosensory field, the polarizing electric field is coherent (i.e. it is similar in time course, but has differences in amplitude) and aligned (the direction of the polarizing field is characteristically the same for a given object's location). This means that the time course of object polarization depends on the intrinsic properties of the object, but is independent of object position and orientation relative to the main axis of the fish body [25]. Thus, in pulse mormyriforms, the polarization of an object encodes the type of material of an object separate from its position and orientation in the field. In fact, while a resistive object in any location in the electrosensory field modulates only in amplitude stimulus profile on the electrosensory mosaic, the polarization of a capacitive object in any place of the electrosensory field modulates both waveform and amplitude stimulus profile. Nonetheless, all possible waveforms generated by a given object's impedance define a family of waveforms that characterize an impedance-related characteristic of the object (referred to as "electric color" by Budelli and Caputi [25]). Consistent with the above hypothesis, there are two types of electrosensory afferents [15, 16, 102], one type encodes the spatial pattern of amplitude, while the other is sensitive to both the amplitude and time course of the stimulus field [99]. The information carried by both types of receptors is processed in parallel in different maps of the electrosensory lobe [12, 15, 16, 63, 67] and probably converge on mesencephalic structures allowing the fish to effectively discriminate "electric color" [49, 50, 97].

4.1.2. Gymnotiformes. In the head region of most gymnotiforms (excluding those having supernumerary EOs, as *Steatogenys elegans*, 17) the percutaneous field is coherent and aligned, but along the rest of the fish's body it shows a stereotyped transcutaneous pattern that sweeps the mosaic from rostral to caudal regions [2, 6, 34, 81, 96]. This duality is explained by our toy model which considers the polarizing field as the weighted sum of the fields generated by individual sources located at different sites with respect to the hemispace limiting plane (equation 1). This predicts that the location of multiple electrogenic sources relative to the body surface, and the differences in the waveforms that they emit, determine the differences both between body regions and between wave and pulse gymnotiforms.

The high coherence and alignment of the polarizing field at the foveal electrosensory field when several poles are perpendicularly aligned to the hemispace limit is due to the small contribution of more distant poles to the polarizing field. The prevalence of the rostral-most regions of the EO in the time course of the field is enhanced by the tapered shape of the caudal-most region of the body typical of gymnotiforms [30, 38].

In the peripheral field, at short distances from the skin, distances between an object and the poles vary reciprocally.

Consequently, when the weighting factor increases for a group of poles it decreases for the rest. This means that, within a short range, the contribution of each pole to the polarizing field varies greatly with object position and movement along the body.

To the sides of wave fish, the polarizing field vector rotates along the time. The poor alignment of the polarizing field is due to the differences in phase. Like in tomographic procedures, the field polarizes the object from different angles, allowing the evaluation of geometrical aspects of the object in more detail [5, 19, 20, 90, 91], and also to be able to easily detect object presence independent of its orientation relative to the fish's main axis. In addition, as pointed out by Scheich and Bullock [87] early on, and more recently studied and applied to man-made systems [9-11], capacitive impedance may cause variations in the stamp phase. In addition, it has been theoretically shown that multisite signals possess information sufficient to efficiently identify the targets, provided that their electrical permittivity is not too small at low frequencies [4-5, 20, 90]. Consistently, wave fish have two types of electroreceptors suitable to differentially evaluate phase and amplitude [46 - 47, 57, 61, 87, 102]. Although phase sensing has an important role in electrocommunication and jamming avoidance [13, 27, 55-56, 62, 88], its role in object evaluation [98] has been poorly studied in electric fish.

In pulse Gymnotiformes the waveform emitted by each EO region is specific to each location, Therefore, object polarization comes not only from different directions, but also with different time courses. Electroreceptors are found in two main types, differently encoding the amplitude and phase spectra of the reafferent signals [12, 29, 61, 78, 83, 102]. This strategy potentially provides the fish the ability to extract information on location, shape and material of an object. Although the capabilities of fish in this respect are still uncertain, in artificial agents multisite and multiwave polarization may be used either to dissect these features, or to enhance sensitivity in the peripheral field. This requires the design of biomimetic sensors tuned to different waveforms.

4.2. The three viewpoints of electrolocation: the scene, the object and the fish.

As in the theatre, electrolocation can be evaluated from different point of view. On one side is the scene, providing the contextual framework [3, 74], and on the other side the observed object and the exploring fish (the actors, whose agonistic roles make sense in the context of the scene, of which they are an inextricable part). Here we introduce a method for the quantitative evaluation of the electrosensory scene and the actors using simple and concrete parameters. The experimental data obtained in five fish showed the same qualitative results for the following: 1) The scene, as seen from a cylindrical object-probe placed at multiple positions and orientations, behaves as a linear system, and therefore can be characterized by a Thevenin equivalent (*Es* and *Rs* [14, 59, 72, 74]). 2) The agonistic role of an object in the "electrosensory play" can be characterized by the concept of stamp. The quantitative evaluation of this concept (ε), facilitated here by employing a kind of cylindrical probe frequently used in behavioral studies, experimentally confirmed toy model predictions. In addition, our results indicate that, in the context electrosensory mosaic literature [12, 38, 61, 69, 102], the electrosensory field of pulse Gymnotiformes has two regions with different functional properties: a peripheral field and a foveal field. 3) The evaluation of the protagonist's behavior when facing changes in one of the object's intrinsic properties (e.g. longitudinal impedance) in different contextual conditions (e.g. position and orientation) confirmed this hypothesis. Our results suggest that the role of the coherent and aligned polarization field exhibited by the foveal electrosensory field allows these fish to separately evaluate, with high resolution, the location and impedance of an object, while the main role of the non-coherent and rotating polarization field on the sides of the fish is used to enhance detection sensitivity for small objects to be further explored in the foveal electrosensory field by reorienting their body [68,71].

4.2.1. The scene. Our experiments suggest that while the effect of the low resistance of the fish body on *Rs* determines a juxtacutaneous "amplification fringe" (exemplified in Figure 6), *Es* (as seen from the bases of the cylindrical probe), provides it with partial information on object location and orientation relative to the fish body. One should recall that in pulse Gymnotiformes the time courses of the regional EODs are site-dependent [31, 39-41, 84-85, 100] and *Es* is the weighted sum of the effects of them. The toy model suggests that, 1) due to the length of the fish's body and the lack of sources on the head region [30, 38, 73] the polarizing field rostral of the head is dominated by the rostral-most regions of the EO and 2) the relative weight of each component of *Es* shows large variation with an object's position along the side of the fish and with the object's orientation relative to the longitudinal axis of the fish. Measurements of *Es* confirm the presence of a field dichotomy: a foveal electrosensory field in which objects are polarized with coherent and aligned fields, and a peripheral electrosensory field in which objects are polarized by rotating electric fields of site-dependent waveforms.

4.2.2. The object. The type of objects used in this study have contributed to the understanding natural electroreception [1, 3, 33, 75, 97, 98] and may mimic objects of potential interest in artificial electroreception. In spite that the probability of finding the in natural environments is low they have the advantage of facilitating the analysis of the scene in a simple way using a Thevenin-Norton approach. The agonistic effect of the object can be calculated from experimental data and expressed quantitatively as the stamp (ε). The changes in ε with the manipulation of an object's orientation and impedance allowed the comparison of the imaging process and the functional characteristics of the foveal and peripheral electrosensory fields.

In the foveal field, the amplitude of the stamp is highly dependent on the object's orientation. At the midline, ε is

maximal when the longitudinal axes of the object and fish body is parallel, but minimal with perpendicular orientations. As the field fans outward, amplitude decays longitudinally, and increases with perpendicular orientation in such a way that the blind spot present when a given object is transversally centered gives way to a rapid change in the object's polarization polarity, and a lateralization of its image on the fovea. This property of the foveal field gives physical support to the well-known tendency of these fish to follow the field lines searching for prey [89] that has bioinspired a successful algorithm of searching and docking described for an artificial electrosensing agent [22-24, 79]. Another property derived from the coherence of the time course observed at the electrosensory field is the ability to map the impedance of the object onto a waveform. This implies that in the foveal field, the rules discussed above for pulse mormyriforms on "electric color" perception can be also applied for pulse gymnotiforms. This matches with the presence of at least two types of receptors on the head of pulse Gymnotiformes, and their differential sensitivity to the amplitude and phase spectra of the stimulus [1, 29, 83].

In the peripheral electrosensory field, objects are polarized differently depending on their position, orientation and impedance. This complex form of polarization appears to enhance object detectability by *G. omarorum* (see below), but could also be used in biomimetic artificial agents to differentially evaluate position, orientation and impedance, provided that they have multiple electrogenic sources, and are possess a variety of waveform-tuned sensors. Interestingly, when the main axes of the object and the fish are orthogonal, the time course of polarization is similar as the fish moves away from the skin along a perpendicular line.

4.2.3. The fish. *Gymnotus omarorum* reacts in the presence of any new sensory stimulus, rapidly increasing the rate of the pacemaker commanding each EOD [1, 26, 101]. Using this "novelty response" we showed that a given fish is able to discriminate between amplitude, and also between waveforms, in the foveal electrosensory field – supporting the possibility of "electric color" detection in the fovea. In the peripheral field, the correlation between the amplitude of the novelty response and the increase in stamp rms value was very poor when positions over the whole peripheral electrosensory field were considered. One possible explanation of this lack of correlation between the increment in stamp and the amplitude of the novelty response in the peripheral electrosensory field is that due to the electric field complexity, changes in resistance imply changes in stimulus waveform. This facilitates omnidirectionality of object detection when it moves in the peripheral field. This does not rule out waveform discrimination on the sides of the body. In fact, novelty responses were present when object impedance was stepped from a capacitive to a resistive load without change in the stamp rms value. Further, there is a good correlation between the increment in an object's stamp and the amplitude of the novelty response when the set of an object's positions is restricted to those along a line perpendicular to the fish's main axis. As shown in Figure 9, while in these positions the amplitude of the stamp decays with distance but waveform remains similar. Moreover, the similarity of the differences between the slopes obtained stepping to similar or to distinct waveforms supports the hypothesis of omnidirectionality, but does not rule out the possibility of "electric color" evaluation on the sides of the body.

4.3. Conclusions.

Pulse Gymnotiformes offer the most complex natural design for object' polarization. Complexities in the EO, the simplicity of the fish's body, and separate systems for controlling mobility [28] allow *G. omarorum* to generate two different regions in the electrosensory field. These regions have functions similar to those observed in the visual field of mammals and birds. There is a foveal field where "colored" images can be evaluated with high spatial resolution, but with large differences in sensitivity for elongated objects oriented at different angles. There is also a peripheral field where objects are polarized from different sites and with different time courses. The latter facilitates object detection independent of its shape and orientation, and triggers searching behaviors that place the object in the foveal field [71].

It is still unclear whether this dual field polarization strategy, including the multisite, multiwaveform approach shown on the side of the fish's body, can be used by a fish to dissect contextual (e.g. position and orientation with respect to the fish's body) and intrinsic (e.g. material, volume, shape) features of an object, or if some of these aspects are fused into object qualia distinct from those recognized in human cognition. Regardless, we hypothesize that the dual electrosensory field organization including the complex polarization strategy exhibited by *G. omarorum* may be applied by artificial agents to separately identify contextual and intrinsic features. This may require developing a proper sensory mosaic specifically designed to evaluate stimulus waveforms, and a repertoire of complex electrosensory guided movements to alternate peripheral and foveal exploration of an object. The challenge is launched.

Acknowledgements

Authors thank Dr. J.C. Waddell for insightful comments and English editing. Partially supported by Programa de desarrollo en Ciencias Basicas (PEDECIBA) and Agencia Nacional de Investigacion e Innovacion, Uruguay.

References

[1] Aguilera PA, Caputi AA, 2003 *Journal of Experimental Biology* **206** 6 989-998

[2] Aguilera PA, Castello ME, Caputi AA, 2001 *Journal of Experimental Biology*, **204** 2 185-198

[3] Aguilera PA, Pereira, AC Caputi AA, 2012 *Journal of Experimental Biology* **215** 9 1533-1541.

[4] Ammari H, Boulier T, Garnier J, 2013 *SIAM Journal on Imaging Sciences*, **6** 1 285–321.

[5] Ammari H, Boulier T, Garnier J, Han W, 2014 *Proceedings of the National Academy of Sciences*, **111** 32 11652–11657.

[6] Assad C, Rasnow B, Stoddard PK, 1999 *Journal of Experimental Biology*, **202** 10 1185-1193
[7] Bacelo J, Engelmann J, Hollmann M, Von Der Emde G, Grant K, 2008 *Journal of Comparative Neurology* **511** 3, 342-359.
[8] Bacher M, 1983 *Biological cybernetics*, **47** 1 51-58.,
[9] Baffet G, Boyer F, and Gossiaux PB, 2009 *IEEE International Conference on Robotics and Biomimetics* 659-664 IEEE.
[10] Bai Y, Neveln ID, Peshkin, M, MacIver MA, 2016 *Bioinspiration & biomimetics*, **11** 5 055001.
[11] Bai Y, Snyder J, Silverman, Y, Peshkin M, MacIver MA, 2012 *IEEE/RSJ International Conference on Intelligent Robots and Systems* 1467-1472.
[12] Bastian J, 1986 *Electrolocation In Electroreception* Bullock TH and Heiligenberg W (eds) . Wiley & Sons, New York 577-612.
[13] Bastian J, Heiligenberg W, 1980 *Journal of Comparative Physiology* **136** 2 135-152.
[14] Bell CC, Bradbury J, Russell CJ, 1976 *Journal of Comparative Physiology* A **110** 65-88.
[15] Bell CC, 1990 *Journal of Neurophysiology* **63** 2 303-318.
[16] Bell CC, 1990 *Journal of Neurophysiology* **63** 2 319–332.
[17] Bennett MVL, Grundfest H, 1959 *Journal of General Physiology* **42** 1067 -1104.
[18] Bennett MVL, 1970 *Annual Review of Physiology* **32** 1 471-528.
[19] Bonnetier E, Triki F, Tsou CH, 2018 *Journal of Mathematical Analysis and Applications*, **464** 1 280-303.
[20] Boulier T, 2013 *Modelling active electrolocation in weakly electric fishes* (Doctoral dissertation, École Polytechnique).
[21] Boulier T, Garnier J, 2013 *SIAM Journal on Imaging Sciences*, **6** 1 285-321.
[22] Boyer F, Gossiaux PB, Jawad B, Lebastard V, Porez M, 2012. *IEEE transactions on robotics*, **28** 2 492-505.
[23] Boyer F, Lebastard V, Chevallereau C, Servagent N, 2013 *IEEE transactions on robotics*, **29** 4 945-956.
[24] Boyer F, Lebastard V, Chevallereau C, Mintchev S, Stefanini C, 2015 *The International Journal of Robotics Research*, **34** 9 1228-1250.
[25] Budelli R, Caputi AA, 2000 *Journal of Experimental Biology* **203** 3 481-492.
[26] Bullock TH, 1969 *Brain, Behavior and Evolution*, **2** 2 , 102-118.
[27] Bullock TH, Hamstra R H, Scheich H, 1972 In *How do Brains Work?* 509-534 Birkhäuser, Boston, MA.,
[28] Caputi AA, 2017 *Bioinspiration & biomimetics* **12** 2 025004.
[29] Caputi AA, Aguilera PA, 2019 *Journal of Experimental Biology*, jeb-191544.
[30] Caputi AA Budelli R 1995 *Journal of Computational Neuroscience* 2 131-147.
[31] Caputi AA, 1999 *Journal of Experimental Biology* **202** 1229 -1241.
[32] Caputi AA, 2004 *Journal of Physiology-Paris* **98** 1-3 81-97.
[33] Caputi AA, Aguilera PA, Castelló ME, 2003 *Journal of Experimental Biology*, **206** 6 999-1010.
[34] Caputi AA, Aguilera PA, Pereira, AC 2011 *PloS one* **6** 8 e22793.
[35] Caputi AA, Aguilera PA, Pereira, AC, Rodríguez-Cattáneo A, 2013 *Brain research*, **1536**, 27-43.
[36] Caputi AA, Carlson BA, Macadar O, 2005 In *Electroreception* 410-451 Springer, New York, NY.
[37] Caputi, ÁA, Castelló ME, Aguilera PA, Pereira, C, Nogueira J, Rodríguez-Cattaneo A, Lezcano C, 2008 *Journal of Physiology-Paris*, **102** 4-6 256-271.
[38] Caputi, ÁA, Castelló ME, Aguilera PA, Trujillo-Cenóz O, 2002 *Journal of Physiology-Paris*, **96** (5-6), 493-505
[39] Caputi A, Macadar O, Trujillo-Cenóz O, 1989 *Journal of Comparative Physiology A* **165** 361–370.
[40] Caputi A, Macadar O, Trujillo-Cenóz O, 1994 *Journal of Comparative Physiology A*, **174** 5 633-642.
[41] Caputi A, Silva A, Macadar O, 1998 *Brain Behaviour Evolution* 52 148 -158
[42] Carr CE, Maler L, Sas E, 1982 *Journal of Comparative Neurology*, **211** 2 139-153.
[43] Castelló M E, Caputi AA, Trujillo-Cenóz O, *1998 Journal of Comparative Neurology*, **401** 4 549-563.
[44] Castelló M E, Aguilera PA, Trujillo-Cenoz O, Caputi AA, 2000 *Journal of Experimental Biology*, **203** 21 3279-3287.
[45] Chen L, House JL, Krahe R, Nelson ME, 2005 *Journal of Comparative Physiology A*, **191** 4, 331-345.
[46] Chacron MJ, Lindner, B, Longtin A, 2004 *Physical review letters* **92** 8 080601.
[47] Chacron MJ, Maler L, Bastian J, 2005 *Nature neuroscience* **8** 5 673.
[48] Dye J, Meyer J, 1986 In: Bullock TH, Heiligenberg W (eds) Electroreception. Wiley, New York 71–102.
[49] Gottwald M, Bott R A, von der Emde G, 2017 Journal of Experimental Biology, **220** 17 3142-3153.
[50] Gottwald M, Singh N, Haubrich A N, Regett S, von der Emde G, 2018 Current Biology **28** 22 3648-3653.
[51] Harder W, Schief A, Uhlemann H, 1964 *Journal of Comparative Physiology A* **48** 3, 302-331.
[52] Heiligenberg W, 1975 *Journal of comparative physiology* **103** 1 55-67.
[53] Heiligenberg W, 1975 *Journal of comparative physiology* **103** 3 247-272.
[54] Heiligenberg W, 1975 *Principles of electrolocation and jamming avoidance in electric fish: a neuroethological approach* (Vol. 1). Springer Science & Business Media.
[55] Heiligenberg W, 1991 *Neural nets in electric fish* Cambridge, MA MIT press.
[56] Heiligenberg W, Baker C, Matsubara J 1978 *Journal of comparative physiology* **127** 3 267-286 .
[57] Hopkins CD, 1976 *Journal of Comparative Physiology*, **111** 2 171-207.
[58] Hopkins CD, 1999 *Journal of Experimental Biology*, **202** 10 1217-1228.
[59] Jackson JD, 1999 *Classical Electrodynamics* (3rd ed.). New York: John Wiley & Sons.
[60] Kawasaki M, 1994 *Journal of Comparative Physiology A*, **174** 2 133-144.
[61] Kawasaki M, 2005 Physiology of tuberous electrosensory systems. In Electroreception. Springer, New York, NY 154-194.
[62] Keller CH, Maler L, Heiligenberg W, 1990 *Journal of Comparative Neurology* **293** 3 347-376.
[63] Krahe R, Maler L, 2014 *Current Opinion in Neurobiology*, **24**, 13-21.
[64] Lissmann HW 1951 *Cuv. Nature* **167** 201–202.
[65] Lissmann HW 1951, *Journal Experimental Biology* **35** 156-191.
[66] Lissmann HW Machin K E 1958 *Journal Experimental Biology* **35** 451-486.
[67] Maler L, 1979 *Journal of Comparative Neurology*, **183** 2 323-363.
[68] Maciver M A, Sharabash NM, Nelson M E 2001 *Journal of Experimental biology*, **204** 3 543-557.
[69] McKibben JR, Hopkins CD, Yager D D 1993 *Journal of Comparative Physiology A*, **173** 4 415-424.

[70] Migliaro A, Caputi AA, Budelli R, 2005 *PLoS computational biology*, **1** 2 e16
[71] Nelson ME, Maciver MA, 1999 *Journal of Experimental Biology*, **202** 10 1195-1203.
[72] Nunez PL, Srinivasan R, 2006 Electric fields of the brain: the neurophysics of EEG Oxford University Press, USA
[73] Pedraja F, Aguilera P, Caputi AA, Budelli R, 2014 *PLoS computational biology* **10** 7 e1003722.
[74] Pereira AC, Caputi AA 2010 *Interdisciplinary Sciences: Computational Life Sciences*, **2** 4 291-307.
[75] Pereira AC, Aguilera P, Caputi AA 2012 *Journal of Experimental Biology* **215** 18 3266-3280.
[76] Pereira AC, Rodríguez-Cattaneo A, Caputi AA 2014 *Journal of Physiology-Paris*, **108** 2-3 71-83.
[77] Pereira A C, Centurión V, & Caputi AA, 2005 *Journal of experimental biology*, *208* 5 961-972.
[78] Rodríguez-Cattaneo A Pereira AC,, and Caputi AA 2017 *Int J Biosen Bioelectron* 2.6 00047.
[79] Porez M, Lebastard V, Ijspeert AJ, Boyer F, 2011 IEEE/RSJ *International Conference on Intelligent Robots and Systems* 1901-1906.
[80] Pusch R, von Der Emde G, Hollmann M, Bacelo J, Nöbel S, Grant K, Engelmann J, 2008 *Journal of Experimental Biology* **211** 6 921-934.
[81] Rasnow B, Bower JM, 1996 *Journal of Comparative Physiology A*, **178** 3 383-396.
[82] Rasnow B, 1996 *Journal of Comparative Physiology A*, **178** 3 397-411.
[83] Rodríguez-Cattaneo A, Aguilera PA, Caputi AA 2017 *Journal of Experimental Biology*, **220** 9 1663-1673.
[84] Rodríguez-Cattaneo A, Aguilera PA, Cilleruelo E, Crampton WGR, Caputi AA 2013 *Journal of Experimental Biology*, **216** 8 1501-1515.
[85] Rodríguez-Cattaneo A, Pereira, AC, Aguilera PA, Crampton, WGR, Caputi AA 2008 *PLoS One*, **3** 5, e2038.
[86] Sawtell NB, Williams A, 2008 *Journal of Neuroscience*, *28*(7), 1598-1612.
[87] Scheich H, Bullock TH, 1974 In *Electroreceptors and Other Specialized Receptors in Lower Vertrebrates* 201-256 Springer, Berlin
[88] Scheich H, Bullock TH, Hamstra Jr, RH 1973 *Journal of Neurophysiology*, **36** 1 39-60.
[89] Schluger JH, Hopkins CD 1987 *Journal of Experimental Biology*, **130** 1 359-367.
[90] Schmidt R, 1986 *IEEE Transactions on Antennas and Propagation* **34** 3 276–280, .
[91] Scholz B, 2002 *IEEE Transactions on Medical Imaging*, **21** 6 588–595.
[92] Servagent N, Jawad B, Bouvier S, Boyer F, Girin A, Gomez F, Gossiaux, PB 2013 *IEEE Sensors Journal*, **13** 5 1865-188.
[93] Shifman AR, Longtin A, Lewis JE, 2015 *Scientific reports* **5** 15780
[94] Sim M, Kim, D 2011 *Journal of Experimental Biology* **214** 14 2443-2450.
[95] Snyder J B, Nelson ME, Burdick JW, MacIver MA. 2007 *PLoS biology*, **5** 11 e301.
[96] Stoddard PK, Rasnow B, Assad C, 1999 *Journal of Comparative Physiology A*, **184** 6 609-630.
[97] von der Emde G, 1990 *Journal of Comparative Physiology A*, **167** 3 413-421.
[98] von Der Emde G, 1998 *Journal of Comparative Physiology A* **182** 2 217-224.
[99] von der Emde G, Bleckmann H, 1997 *Journal of Comparative Physiology A* **181** 5 511-524.
[100] Waddell JC, Rodríguez-Cattáneo A, Caputi AA, Crampton WG 2016 *Journal of Physiology-Paris* **110** 3 164-181.
[101] Westby G W M 1975 *J. Comp. Physiol.* **96**, 307–341.
[102] Zakon H 1986 *The electroreceptive periphery In Electroreception* Bullock TH and Heiligenberg editors, Wiley NY.